# Properties of single and multiple defect modes in one-dimensional photonic crystals containing left-handed metamaterials

**Munazza Zulfiqar Ali**

*Physics Department, Punjab University, Lahore, Pakistan*

*Corresponding author: munazzazulfiqar@yahoo.com*

Received November 28, 2011; accepted February 24, 2012; posted online May 9, 2012

Wave propagation is studied in structures consisting of alternate left- and right-handed layers. Bragg gap and zero-n gap appear in different frequency regions of the structure. The periodicity of the structure is broken by simply reversing the order of the layers in one half of the structure, resulting in defect modes located inside the zero-n gap and Bragg gap. These modes can be made very narrow by adding more layers in the structure. The defect mode located inside the zero-n gap is sensitive to the symmetry of the structure and insensitive to the angle of incidence of the incoming radiation. Multiple modes are also generated inside the gaps by repeating the structural pattern. Thus, a simple structure can be used for single and multiple modes that are important for different applications.

*OCIS codes:* 160.5298, 160.3918.

*doi: 10.3788/COL201210.071604.*

Metamaterials refer to artificial composite structures, whose properties are beyond those of usual materials[1−7]. These structures comprise a homogenous medium for the working wavelength. Left-handed metamaterial (LHM) refers to a medium, in which the electric permittivity and magnetic permeability simultaneously have a negative value over a certain frequency range. The LHMs have been experimentally realized by combining the permittivity negative and the permeability negative metamaterials. The former have been realized in the form of three-dimensional (3D) array of very long, thin continuous wires in which cuts are periodically introduced[2,6,7], whereas the latter have been realized in the form of splitring resonators[3,6,7].

The inclusion of LHMs in photonic band gap (PBG) structures has led to the emergence of new mechanisms to produce photonic gaps[8−15]. In the conventional PBG structures, the Bragg gaps result from the multiple interference mechanism. As a result, their central frequency is highly sensitive to the geometrical scaling of the structure as well as to the angle and polarization of the incident light. In a one-dimensional (1D) PBG structure containing alternate left-handed and regular material (also called right-handed) layers, the volume averaged refractive index of the structure becomes zero over a certain frequency range. Such a frequency range cannot support propagating modes and has been termed as a zero-n gap[8,13,14]. Given that zero-n gap does not result from the interference phenomenon, it has quite distinct properties compared with that of the Bragg gap. Zero-n gap is also relatively insensitive to geometrical scaling of the structure and angular change and polarization of the incident radiation[16]. Many suggestions have been made to utilize such properties for practical applications[17−20]. One way is to introduce defect modes in zero-n gaps. The concept of the defect mode in PBG structures is very similar to impurity states in semiconductors. Defect modes are produced by introducing some kind of irregularity in a PBG structure. This break in the periodicity of the structure may produce a transmitting mode within the forbidden region of propagation. Such a propagating mode located inside the gap is known as the defect mode[21]. Defect modes are important for their potential applications. These are utilized in making filters and mode selectors, which are important components in optical communication and electro-optical systems. In this letter, we study a simple structure that gives rise to defect modes. In this scheme, there is no need to introduce any extra layer; the periodicity of the structure is broken by simply reversing the order of the layers in one half of the structure. Such a structure has been referred to previously as a conjugated photonic crystal (PC), and the properties of defect modes in conjugated PC consisting of regular materials have been studied in Ref. [22]. In this letter, we examined the properties of defect modes in conjugated PCs, in which alternate layers consisted of left-handed and regular materials. Previously, only single mode has been studied[22]. We also find that the repetition of the structure gives rise to multiple modes. In the structure considered, the number of modes simply depends on the number of conjugated PCs. Different characteristics of single and multiple modes have also been studied.

A periodic structure consisting of two layers A and B is considered (Fig. 1); in our structure, A is a LHM layer, and B is a regular material layer. The electric permittivity $\varepsilon(\omega)$ and the magnetic permeability $\mu(\omega)$ of the LHM layer are represented by the Drude model given by

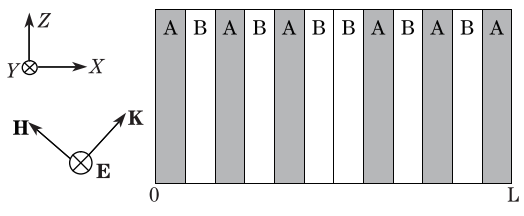


Fig. 1. Schematic diagram of the $(AB)^3(BA)^3$ structure under consideration.

 

$$\varepsilon_{\rm A}(\omega) = 1 - \frac{10}{\omega(\omega + {\rm i}\gamma)}, \quad \mu_{\rm A}(\omega) = 1 - \frac{10}{\omega(\omega + {\rm i}\gamma)}, \tag{1a}$$

$$\varepsilon_{\rm B} = 2.5, \quad \mu_{\rm B} = 1, \tag{1b}$$

where $\omega$ is the frequency of the incident radiation, and $\gamma$ is the damping coefficient. The LHM are always lossy. The effect of losses is that they damp the magnitude of the transmitting modes[23,24]. The focus of the present study is to compare different characteristics of the defect modes located inside the zero-n gap and the Bragg gap. Here, losses are assumed to be absent similar to previous studie[10]; however, these can be included and can result in relatively decreased magnitude of the transmitting modes. The transfer matrix approach was used to study wave propagation through the structure. The transfer matrix for the $j$th layer can be written as

$$\mathbf{m}_j = \begin{bmatrix} \cos k_j d_j & -\dfrac{1}{q_j}\sin k_j d_j \\ q_j \sin k_j d_j & \cos k_j d_j \end{bmatrix}, \tag{2}$$

where

$$q_j = \frac{\sqrt{\varepsilon_j}}{\sqrt{\mu_j}}\sqrt{1 - \frac{\sin^2\theta}{\mu_j \varepsilon_j}} \quad . \tag{3}$$

In Eq. (3), $k_j$ and $d_j$ represent the local wave vector and width corresponding to the $j$th layer, respectively, and $\theta$ represents the angle of incidence. The tangential components of the electric and magnetic fields at the incident side $x = 0$ and at the transmitted side $x = L$ are related by:

$$\begin{bmatrix} E_1 \\ H_1 \end{bmatrix}_{x=0} = \mathbf{M} \begin{bmatrix} E_N \\ H_N \end{bmatrix}_{x=L}, \tag{4}$$

$$\mathbf{M} = \prod_{j=1}^{N+1} m_j, \tag{5}$$

where, $N$ represents the total number of layers in the structure. The transmission coefficient $T$ of the finite structure is calculated by applying the boundary conditions at the incident and the transmitted ends, and is given by the following expression:

$$T = \frac{2q_0}{[(q_0\mathbf{M}_{11} + q_0\mathbf{M}_{22}) - (q_0^2\mathbf{M}_{12} + \mathbf{M}_{21})]}, \tag{6}$$

where $q_0 = \sqrt{1 - \frac{\sin^2\theta}{\varepsilon_0\mu_0}} = \cos\theta$, because there is air on

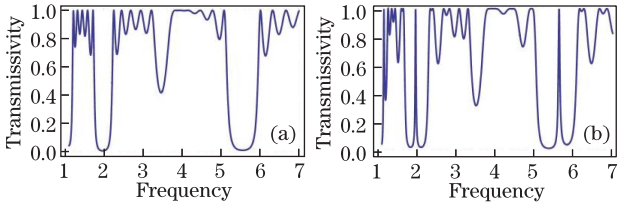


Fig. 2. (a) Transmission versus frequency graph of the $(AB)^6$ structure shows the zero-n gap in the frequency region $1.8 < \omega < 2.1$ and the Bragg gap in the frequency region $5.1 < \omega < 6$. (b) The transmission versus frequency graph of the $(AB)^3(BA)^3$ structure, defect modes appear in the zero-n gap and the Bragg gap.

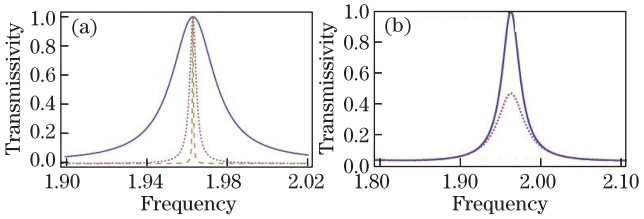


Fig. 3. Transmission versus frequency graph. (a) Solid, dashed and the dotted graph correspond to $(AB)^3(BA)^3$ , $(AB)^4(BA)^4$ , and $(AB)^5(BA)^5$. (b) The solid and the dotted lines correspond to the $(AB)^3(BA)^3$ and $(AB)^2(BA)^4$ structure.

the incident and the transmitted sides of the structure, and $\mathbf{M}_{\rm lm}$ represents the elements of the matrix $\mathbf{M}$.

Dimensionless units have been used in the calculations, i.e., $\omega = \frac{\omega' d}{c}$ is the dimensionless frequency ($\omega'$ being frequency in real units, and $c$ is the velocity of light) and $D_{\rm A} = \frac{d_{\rm A}}{d}, D_{\rm B} = \frac{d_{\rm B}}{d}$ are the dimensionless widths of the layers (where $d = d_{\rm A} + d_{\rm B}$).

Initially, we considered wave propagation in a periodic structure ABAB without any irregularity. The transmissivity versus frequency plot of this structure is shown in Fig. 2(a), which features a structure comprising 6 AB periods. For the $\omega < \sqrt{10}$, layer A has a negative refractive index and behaves as a LHM. A zero-n gap appears in the frequency region $1.8 < \omega < 2.1$. In this frequency region, the average refractive index of the structure defined by $n_{\rm av} = n_{\rm A}D_{\rm A} + n_{\rm B}D_{\rm B}$, becomes zero. A Bragg gap appears in the frequency region $5.1 < \omega < 6$, where both the layers have positive refractive indexes. Figure 2(b) shows the transmissivity versus frequency plot of a structure, in which the order of the layers in the last three periods has been reversed, i.e., this PC can be written as $(AB)^3(BA)^3$. This structure can also be regarded as a combination of two conjugated PCs. The periodicity of the structure is broken in this way, after which the defect modes appear both in the zero-n gap and the Bragg gap (Fig. 2(b)). The main advantage of the structure lies in the fact that there is no need to introduce some extra layer or change structure parameters; instead, the periodicity of the structure is broken by simply reversing the order of growth of the layers. As the properties of such a defect mode in Bragg gap have already been investigated[22], we only focused on the properties of the defect mode that are located inside the zero-n gap. Figure 3(a) shows how the width of the mode changes by increasing the number of periods in the structure. The mode can be made very narrow by increasing the number of periods in the structure. It is noteworthy that a defect mode is created inside the gaps just by reversing the order of the layers; moreover, the confinement effect grows very effectively and the width of the mode decreases very rapidly by adding few more periods. In this way, the quality factor of the mode is enhanced many times. The quality factor is very important if the mode is to be utilized for making filters; in addition, the mode is sensitive to the symmetry of the structure. In Fig. 3(b), the solid line corresponds to the $(AB)^3(BA)^3$ structure, which gives rise to a mode of transmission coefficient 1, whereas the dotted line corresponds to the $(AB)^2(AB)^4$ structure, which gives rise to a defect mode of transmis-

sion coefficient nearly equal to 0.4. The mode disappears as the structure is made more asymmetrical. Figure 4 shows the dependence of the defect modes on the angle of the incident radiation. The defect mode in the zero-n gap is almost insensitive to the angular change of the incident radiation, whereas the defect mode in the Bragg gap shifts on the frequency scale considerably as the angle of the incident radiation is changed. Both properties can be utilized in certain applications. The insensitivity of the zero-n defect mode can be utilized in making omnidirectional applications. The modes located inside the Bragg gap can be used in making angle tunable filters.

Figure 5(a), which shows modes inside the zero-n gap only, demonstrates the transmission spectrum of the $(AB)^3(BA)^3(AB)^3$ structure. This structure provides two interfaces where the waves become localized; hence, two defect modes appear inside the gaps. Next, Fig. 5(b) shows the transmission spectrum of the $(AB)^3(BA)^3(AB)^3(BA)^3$ structure, in which three defect modes appear inside the zero-n gap. Repeating the pattern, the number of defect modes inside the keeps increasing, as shown in Figs. 5(c) and (d), where four and five modes appear in the transmission spectra corresponding to the $(AB)^3(BA)^3(AB)^3(BA)^3(AB)^3$ and $(AB)^3(BA)^3(AB)^3(BA)^3(AB)^3(BA)^3$ structures, respectively.

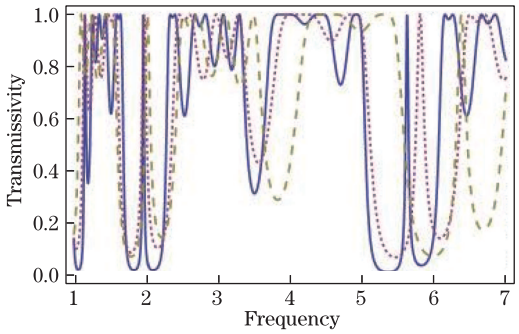


Fig. 4. Angular dependence of the defect mode in the zero-n gap and in the Bragg gap. The solid, dotted, and dashed curves correspond to the angles of incidence of $0°, 30°$, and $45°$, respectively.

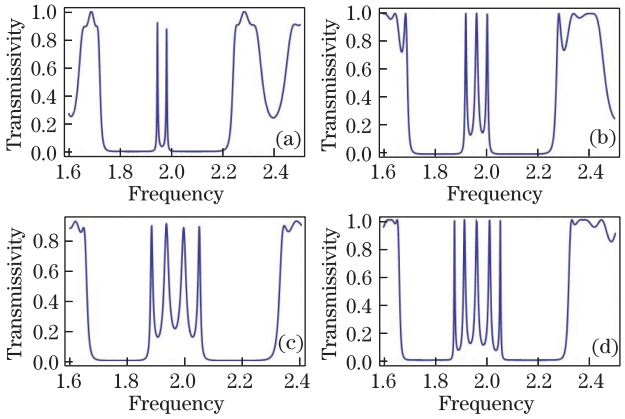


Fig. 5. Appearance of multiple modes in the zero-n gap. (a) $(AB)^3(BA)^3(AB)^3$, (b) $(AB)^3(BA)^3(AB)^3(BA)^3$, (c) $(AB)^3(BA)^3(AB)^3(BA)^3(AB)^3$, and (d) $(AB)^3(BA)^3(AB)^3(BA)^3(AB)^3(BA)^3$.

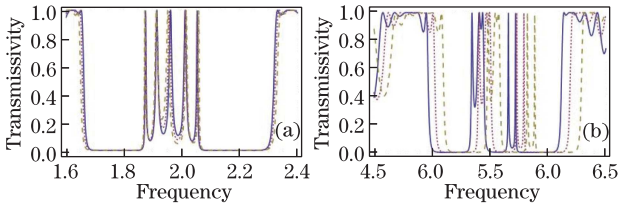


Fig. 6. (a) Multiple modes in the zero-n gap are relatively insensitive to the incidence angle, whereas in (b) the modes located inside the Bragg gap depend strongly on the incidence angle. The solid, dotted, and dashed curves correspond to the angles of incidence of $0°, 30°$, and $45°$, respectively in both (a) and (b) parts.

The properties of these multiple modes can be investigated in the same way as that done for a single mode. Here, we investigated only the angle dependence of these multiple modes. Figure 6(a) shows the angular dependence of the multiple modes located inside the zero-n gap, whereas Fig. 6(b) shows the angular dependence of the modes inside the Bragg gap. The modes inside the zero-n gap are shown to be nearly insensitive to the angular dependence, whereas those inside the Bragg gap shift drastically on the frequency axis as the angle of the incident radiation is changed.

In conclusion, the appearance and properties of single and multiple modes are investigated in a simple structure containing positive and negative refractive index layers. The periodicity of the structure is broken by simply changing the order of the A and B layers of the structure in order to introduce defect modes. These modes can be made very compact by adding more layers in the structure. Modes inside the zero-n gap show angular insensitivity, whereas those inside the Bragg gap show angular dependence. Both properties can be utilized.

## References

1. V. G. Veselago, Sov. Phys. Usp. **10,** 509 (1968).
2. J. B. Pendry, A. J. Holden, J. Stewart, and I. Yungs, Phys. Rev. Lett. **76,** 4773 (1996).
3. J. B. Pendry, A. J. Holden, D. J. Robbins, and W. J. Stewart, IEEE Trans. Microw. Theory Technol. **47,** 2075 (1999).
4. J. B. Pendry, Phys. Rev. Lett. **85,** 3966 (2000).
5. R. W. Ziolkowski and E. Heyman, Phys. Rev. E **64,** 056625 (2001).
6. D. R. Smith, W. J. Padilla, D. C. Vier, S. C. Nemat-Nasser, and S. Schultz, Phys. Rev. Lett. **84,** 4184 (2000).
7. R. A. Shelby, D. R. Smith, and S. Schultz, Science **292,** 77 (2001).
8. R. Ruppin, Microw. Opt. Technol. Lett. **38,** 494 (2003).
9. H. Jiang, H. Chen, H. Q. Li, Y. Zhang, J. Zi, and S. Y. Zhu, Phys. Rev. E **69,** 066607 (2004).
10. L. G. Wang, H. Chen, and S. Y. Zhu, Phys. Rev. B **70,** 245102, (2004).
11. L. Gao and C. J. Tang, Phys. Lett. A **322,** 390 (2004).
12. M. Z. Ali and T. Abdullah, Phys. Lett. A **351,** 184 (2006).
13. R. S. Hegde and H. G. Winful, Opt. Lett. **30,** 1852 (2005).
14. T. Pan, C. Tang, L. Gao, and Z. Li, Phys. Lett. A **337,** 473 (2005).

15. A. Alu and N. Engheta, IEEE Trans. Antennas Propag. **51,** 2558 (2003).
16. J. A. Monsoriu, R. A. Depine, M. L. Martinez-Ricci, and E. Silvestre, Opt. Express **14,** 12958 (2006).
17. P. Li and Y. Liu, Phys. Lett. A **373,** 1870 (2009).
18. T. Tang, W. Liu, X. He, and J. Yang, Opt. Laser Technol. **43,** 1016 (2011).
19. Y. Xiang, X. Dai, S. Wen, and D. Fan, Opt. Lett. **33,** 1255 (2008).
20. W. Rao, Y. Song, and C. Jin, J. Opt. Soc. Am B **27,** 10 (2010).
21. S. G. Johnson and J. D. Joannopoulos, *Photonic Crystals*: *the Road from Theory to Practice* (Springer, German, 2002).
22. L. Tang, L. Gao, and J. Fang, Chin. Opt. Lett. **6,** 201 (2008).
23. A. Yanai, M. Orenstein, and U. Levy, Opt. Express **20,** 3693 (2012).
24. T. Tang, X. Zhong, and W. Liu, Optik **122,** 1832 (2011).